Journal of Materials Science: Materials in Electronics (2020) 31:9065–9075
https://doi.org/10.1007/s10854-020-03490-9

REVIEW

New approach for synthesis of nano-sized $CaCu_3Ti_4O_{12}$ powder by economic and innovative method

R. M. Ramadan[1,3] · Ahmad M. Labeeb[1,2] · Azza A. Ward[1] · Ahmed M. H. Ibrahim[3,4]

Received: 19 January 2020 / Accepted: 25 April 2020 / Published online: 14 May 2020

Abstract

In this work, calcium carbonate ($CaCO_3$), copper oxide (CuO) and titanium oxide (TiO_2) were used as precursors to synthesize nano-sized calcium copper titanate $CaCu_3Ti_4O_{12}$ (CCTO) powder using environmental friendly and modified sonochemical-assisted process. The precursor mixtures were sonicated at 80 °C for 4 h to get a fully precipitated and homogenous product. A pure phase of CCTO powder was obtained at 900 °C. Various techniques were employed to study the phase formation and structural aspects of the calcined CCTO such as XRD, FTIR, HRTEM, TGA and dielectric spectroscopy. The XRD results confirm the formation single phase with cubic structure of the CCTO phase. The absorption bands in FTIR at 400–700 cm^{-1}, which arise from the mixed vibrations of CuO_4 and TiO_6 groups, are prevailing in the CCTO structure. Moreover, the HR-TEM micrographs reveal a highly oriented single cubic crystal structure of particle size ~ 4.78 nm. In addition, the dielectric study discloses that the dielectric constant ε′ increased with increasing the calcination temperature up to 900 °C escorted by a decrease of loss factor (tanδ). This can be attributed to the formation of pure CCTO phase and the highly dense microstructure at high temperatures. Giant dielectric constant ε′ up to (10^6–10^5) exhibited at low frequency (1–1000 Hz). It is deduced that the optimum calcination temperature of the prepared CCTO must not exceed the temperature range (800–900 °C). Furthermore, the prepared CCTO nanopowder is a promising material for energy storage applications.

1 Introduction

Ceramic capacitors characterized by a high speed (charge/discharge) rate and good engineering properties are promising candidates compared to other energy storage devices. The current challenge is to find ceramic capacitors with outstanding storage and good physical properties over a wide temperature range. Perovskite groups of the type (ABO3) such as Barium titanate $BaTiO_3$ and Lead titanate ($PbTiO_3$) exhibited a good dielectric property valuable for capacitor and energy storage applications [1, 2]. But unfortunately, they are non-environment friendly materials [3, 4]. So, seeking for ecofriendly perovskite with stable properties is vital to these applications.

Since 2000 calcium copper titanate perovskite with the formula $CaCu_3Ti_4O_{12}$ (CCTO) has found widespread applications in capacitors, antennas, microwave devices, filters, and sensors. Long ago CCTO has gained a good reputation as a giant dielectric constant material ($\varepsilon' \sim 10^{4-5}$) that is practically stable over a broad temperature range (100–600 K) with good thermal stability [5]. Nearly all studies have attributed the giant ε' value to the Maxwell–Wagner effects at the interface of grains and grain boundaries and electrode polarization effects [6–9].

It is well-known that the electric properties can be remarkably enhanced when ceramic material has a uniform microstructure [10]. For many technological applications as capacitors, resonators and power storage, extremely high dielectric constants and low loss tangents are required. The giant dielectric constants permit miniaturization of the embedded components. This makes it easy for the manufacturers to reduce the size of electronic devices [11].

✉ R. M. Ramadan
rm.mahmoud@nrc.sci.eg; r.mm.ramadan@gmail.com

1 Microwave Physics and Dielectrics Department, Physics Research Division, National Research Centre, 33 EL Bohouth St. Dokki, Giza 12622, Egypt

2 Chemical Physics Interdisciplinary Program, Liquid Crystal Institute, Kent State University, Kent, OH 44242, USA

3 Glass Research Group Physics Department, Faculty of Science, Mansoura University, Mansoura 35516, Egypt

4 Institute of Materials and Machine Mechanics, Slovak Academy of Sciences, Dubravska cesta 9, 84513 Bratislava, Slovakia

Broad innovative work has been done to synthesize $CaCu_3Ti_4O_{12}$. Despite high cost for synthesizing CCTO, some routes faced difficulties to meet the required applications. Several processing routes were adopted for synthesizing CCTO such as solid-state reaction, wet chemistry, sol–gel, solution combustion synthesis, sonochemical, co-precipitation and microwave-assisted routes [12–18]. The solid-state reaction is a conventional route for synthesizing CCTO from $CaCO_3$, CuO, and TiO_2 at high temperatures. But this method is accompanied by some drawbacks like heterogeneity of resultant CCTO and long reaction time. Additional drawbacks are the presence of secondary phases emerged at some stages in the synthesis as a result of limited atomic diffusion through micro-grains [19, 20]. However, some other routes managed to synthesis a homogeneous and high-quality $CaCu_3Ti_4O_{12}$ powder. But they are environmental hazards or contaminated [13, 17].

Late, sonochemical route proved to be a simple and green approach for nanoparticles' synthesis [21–23]. On the whole, this method proceeds in three stages including formation, development and finishes with implosive breakdown of bubbles. An earlier sonochemical-assisted method for synthesizing $CaCu_3Ti_4O_{12}$ (CCTO) was developed by Wongpisutpaisan et al. [16]. In this method, copper nitrate trihydrate ($Cu(NO_3)_2.3H_2O$) and titanium (IV) isopropoxide ($Ti[C_{12}H_{28}O_4$) were used as preliminary materials, then mixed with calcium nitrate trihydrate ($Ca(NO_3)_2{\cdot}0.4H_2O$) after drying at 200 °C. Three different $Ca:Cu_3Ti_4$ compositions (0.75:1, 1:1, 1.25:1) were used to prepare CCTO. The composition 1:1 reveals a giant dielectric constant (10^4) at low frequency and crystallite size ~ 75 nm.

This work aims to prepare a pure phase of $CaCu_3Ti_4O_{12}$ (CCTO) nanoparticles at a relatively low temperature using environmentally clean and modified sonochemical synthesis. $CaCO_3$, CuO and TiO_2 are used as precursors. In addition, XRD, FTIR, TGA, HR-TEM and dielectric properties of CCTO ceramic synthesized by modified sonochemical-assisted process are reported and discussed in detail.

2 Experimental methodology

2.1 Synthesis of nano-sized CCTO

Ultrasonically assisted hydrothermal method has been utilized as a clean and cost-effective approach for the synthesis of $CaCu_3Ti_4O_{12}$ (CCTO) nanopowder with improved chemical and microstructural homogeneity. This approach is environmentally friendly as we have only used raw materials (carbonates and oxides) in addition to distilled water and no additional chemicals or solvent have been used.

The raw materials used in the experiment were calcium carbonate ($CaCO_3$) from [May&Baker (M&B) Degenham Englend] (99%), copper oxide (CuO) from [May&Baker (M&B) Degenham Englend] (98%) and titanium oxide (TiO_2) from Aldrich (USA) (99.99%), respectively. Synthesis of CCTO nanopowder is carried out according to Eq. (1)

$$CaCO_3 + 3CuO + 4TiO_2 \rightarrow CaCu_3Ti_4O_{12} + CO_2 \uparrow . \quad (1)$$

First, appropriate amounts of the precursors (i.e., 1:3:4 stoichiometric ratios of Ca:Cu:Ti ions) according to Eq. 1 were well mixed and partially dissolved into distilled water for 10 min with the help of a magnetic stirrer. Then, the mixture was transferred to ultrasonic bath (Model XN-DTC-27J) adjusted at 80 °C and being sonicated for 4 h. Unlike sonochemical-assisted process [16], the relatively long-time (4 h) procedures are done to complete chemical reactions for achieving a homogenous endproduct. After that, the mixture was filtered and the formed precipitate powder was washed in de-ionized water, and dried at 120 °C for 5 h in an electrical oven. Eventually, to produce CCTO nanoparticles in the ultimate form and attain a full crystallization growth, the desiccated powder was calcined at specified temperatures 600, 700, 800, 900 and 1000 °C for 2 h and then the calcined product was milled using a ball milling to the nano-sized form. The steps of synthesis process of CCTO are schematically illustrated in Fig. 1.

2.2 Techniques

X-ray diffraction patterns of CCTO were studied by Empyrean Panalytical X-ray diffractometer equipped with CuK_α radiation (1.5406 Å) using a step scanning mode, with intervals of 0.02° of 2θ for angular range 3 to 100° and step time 20 s/step. The particle size and electron diffraction patterns of CCTO were examined with high-resolution transmission electron microscope JEOL JX 1230 (HRTEM) and obtained electron diffraction patterns (EDP). Microstructural and characterization of ceramic samples were investigated by employing a scanning electron microscope (SEM), model JEOL-JSM-6510 LV with energy dispersive spectroscopy (EDS) unit. Infrared spectra of CCTO samples calcined at different temperatures were recorded on a JASCO FTIR 300 E Fourier transform infrared (FTIR) spectrometer with a resolution of 2 cm^{-1}. Thermogravimetric analysis TGA was performed using PerkinElmer Thermogravimetric Analyzer (Waltham, MA) USA. Aluminum pans were used, with initial sample mass of about 8–10 mg. The samples were heated from 25 to 1200 °C at a heating rate of 10 °C/min under nitrogen atmosphere.

Dielectric measurements, the samples were pressed and sandwiched between two cupper electrodes. Electrical properties have been investigated using a computer-controlled impedance analyzer (Schlumberger Solartron 1260). The permittivity ε', loss factor tanδ and ac-resistance R_{ac} were

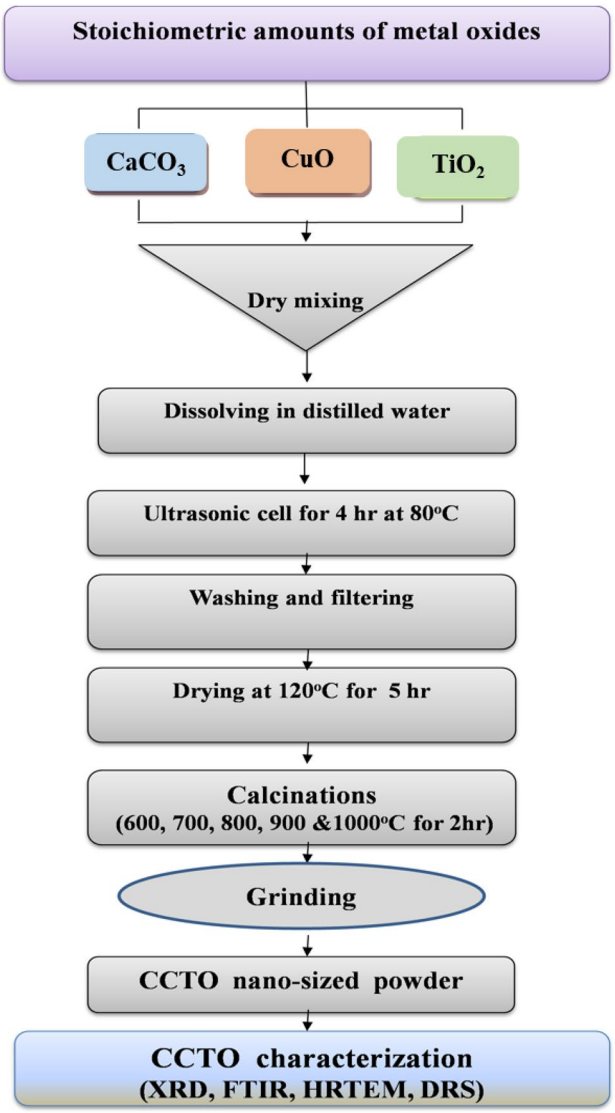

Fig. 1 A flow chart showing the various stages followed for the preparation of CCTO

measured at room temperature ~ 30 °C in a broad frequency range (0.1 Hz–1 MHz). The measurement was automated by interfacing the impedance analyzer with a personal computer through a GPIB cable IEE488. A commercial interfacing and automation software (Lab VIEW) was used for acquisition of data. The error in ε' and tanδ amounts to $\pm 1\%$ and $\pm 3\%$, respectively. The temperature of the samples was controlled by a temperature regulator with Pt 100 sensor. The error in temperature measurements amounts ± 0.5 °C. To avoid moisture, the samples were stored in desiccators in the presence of silica gel. Thereafter, the sample was transferred to the measuring cell and left with P_2O_5 until the measurements were carried out. The reproducibility of the measurement was tested by re-measuring ε' and tanδ after performing the experiment once again.

3 Results

CCTO precursor powder was calcined at different temperatures (600, 700, 800,900 and 1000 °C) for 2 h. The output calcined powder was used to determine the weight loss of the prepared sample as shown in Fig. 2.

Figure 3 presents the TGA curves of the prepared CCTO precursor. It is measured between 100 and 1200 °C in air with a heating rate of 10 °C/min.

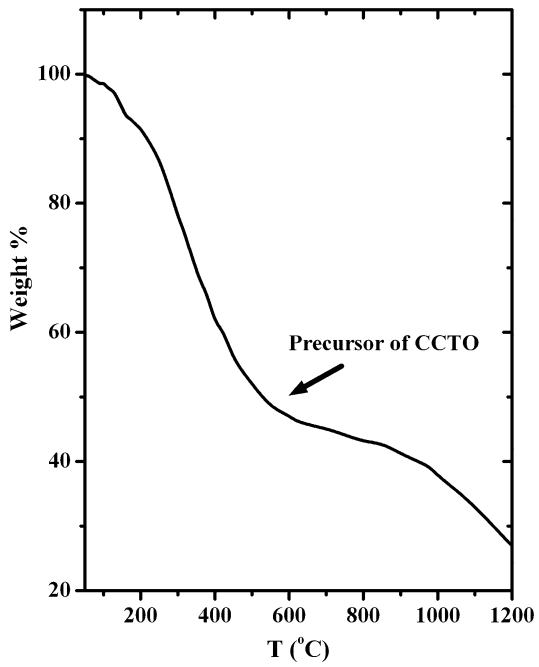

Fig. 2 TGA curves of the thermal decomposition of CCTO heated in air with a heating rate of 10 °C per minute

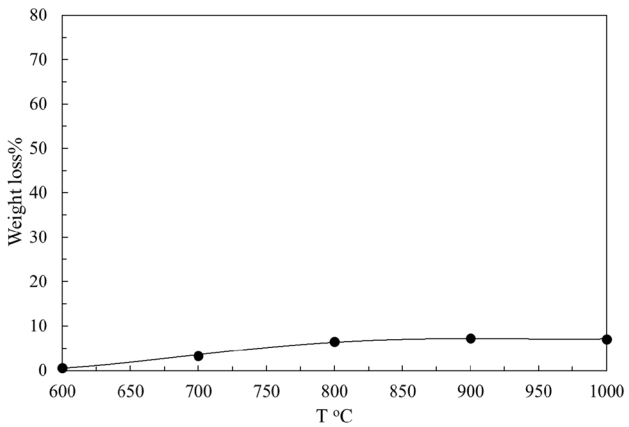

Fig. 3 The change in weight (%) as a function of calcined temperatures of CCTO for 2 h in oven

Figure 4 demonstrates the main diffraction peaks of as-prepared and all calcined CCTO powders at different temperatures, which indicate progressive crystallization with increasing temperature, are comparable to those of the standard powder XRD pattern.

Figures 5 and 6 show scanning electron micrographs (SEM) and EDX spectrum of the surface of CCTO, respectively. All micrographs have the same magnification (×80,000).

The morphology of the CCTO powder calcined at 900 °C was also investigated and the photographs of HR-TEM reveal ab nano-cubic crystal structure of $CaCu_3Ti_4O_{12}$ nanoparticles as clearly seen from Fig. 7.

The corresponding selected area electron diffraction (SAED), which confirms highly oriented cubic crystal structure of the CCTO nanoparticles, is illustrated in Fig. 8.

The FTIR spectra of CCTO powder calcined at different temperatures are illustrated in Fig. 9. For the precursor CCTO, the absorption peak corresponding to 3422 cm^{-1} is related to O–H stretching, while the absorption peak at 1600 cm^{-1} corresponds to the bending mode of H_2O [20]. In addition, the absorption peak in the lower wavenumber 683 and 509 cm^{-1} is due to (X–O) stretch where X = Ti or Cu [21]. The absorption peak at ~ 3440 cm^{-1} disappeared in FT IR spectra for CCTO calcined samples between 600 and 800 °C.

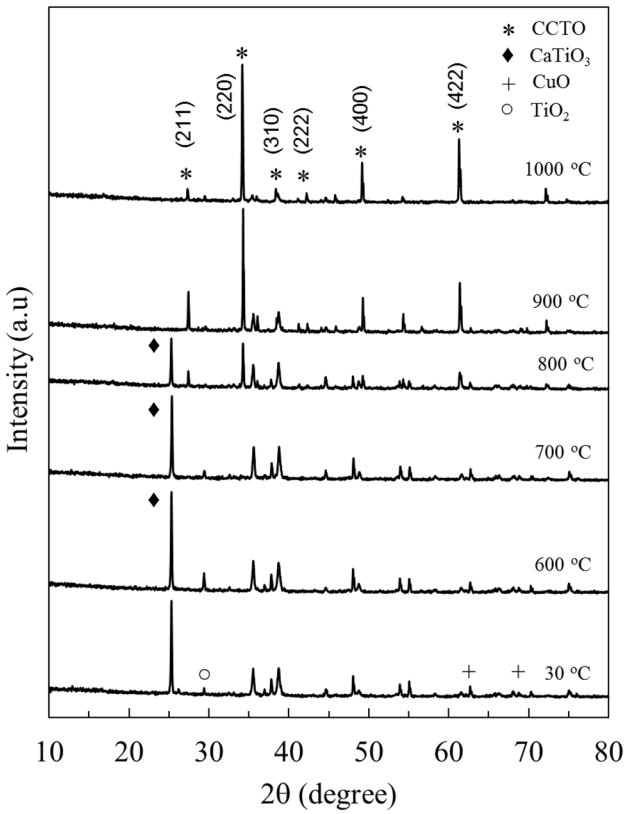

Fig. 4 XRD patterns of CCTO calcined for 2 h in oven at different temperatures

Figure 10 shows the relative area for two regions as a function of calcination temperature.

The dielectric constant ε' and loss factor tanδ for CCTO are represented in Fig. 11 vs. frequency and at room temperature (30 °C). The dielectric constant ε' increased with increasing the calcination temperature up to 900 °C accompanied by a decrease of loss factor (tanδ).

The conductivity vs. calcination temperature is illustrated in Fig. 12. The semi-conductive nature of the grains may arise from a small amount of oxygen loss during ceramic processing in air at elevated temperatures.

4 Discussion

The thermogravimetric curves (TGA) of the prepared powder are depicted in Fig. 2. The TGA curve showed a weight loss of about 7% at 165 °C. At 250 °C the thermal events are associated with the remove of any impurity involved in the prepared powder such as CO_2 and hydroxyl groups [24]. The residual weight is 45% in the temperature range from 150 to 600 °C and it may be due to the decomposition of copper oxide, calcium carbonate and titanium oxide and formation of CuO, $CaTiO_3$ which is confirmed by the XRD for samples calcined at 600–700 °C (will be discussed in details later). From 600 to 1200 °C the residual weight is 27%. However, the material starts to melt at temperature ≥ 1000 °C.

The obtained powder usually needs to be heat treated to remove residual components and being stabilized. So, the weighed CCTO precursor (W_o) powder was calcined at different temperatures (600, 700, 800, 900 and 1000 °C) for 2 h, respectively. Then calcined powder was weighed (W_f) to determine the weight loss (%) according to Eq. 2;

$$\text{Weight loss } (\%) = \left[\frac{(W_o - W_f)}{W_o}\right] \times 100 \quad (2)$$

where W_o is the initial weight and W_f the weight after calcination. The weights were measured to an accuracy of 10^{-4} g. The obtained data are depicted in Fig. 3. At the first region (600–800 °C), the rate of dissociation of CCTO precursor powder increased upon rising calcination temperature. This is due to the removal of moisture and most of the carbon dioxide. However, no significant increase is noticed on reaching (800–1000 °C). The weight loss reached to steady state after losing ~ 70% of the initial weight. This plateau is attributed to the formation of stable phase of CCTO and agrees with TGA results.

Figure 4 presents the main diffraction peaks of all sintered CCTO powders which are comparable to those of the standard powder XRD pattern of cubic phase $CaCu_3Ti_4O_{12}$

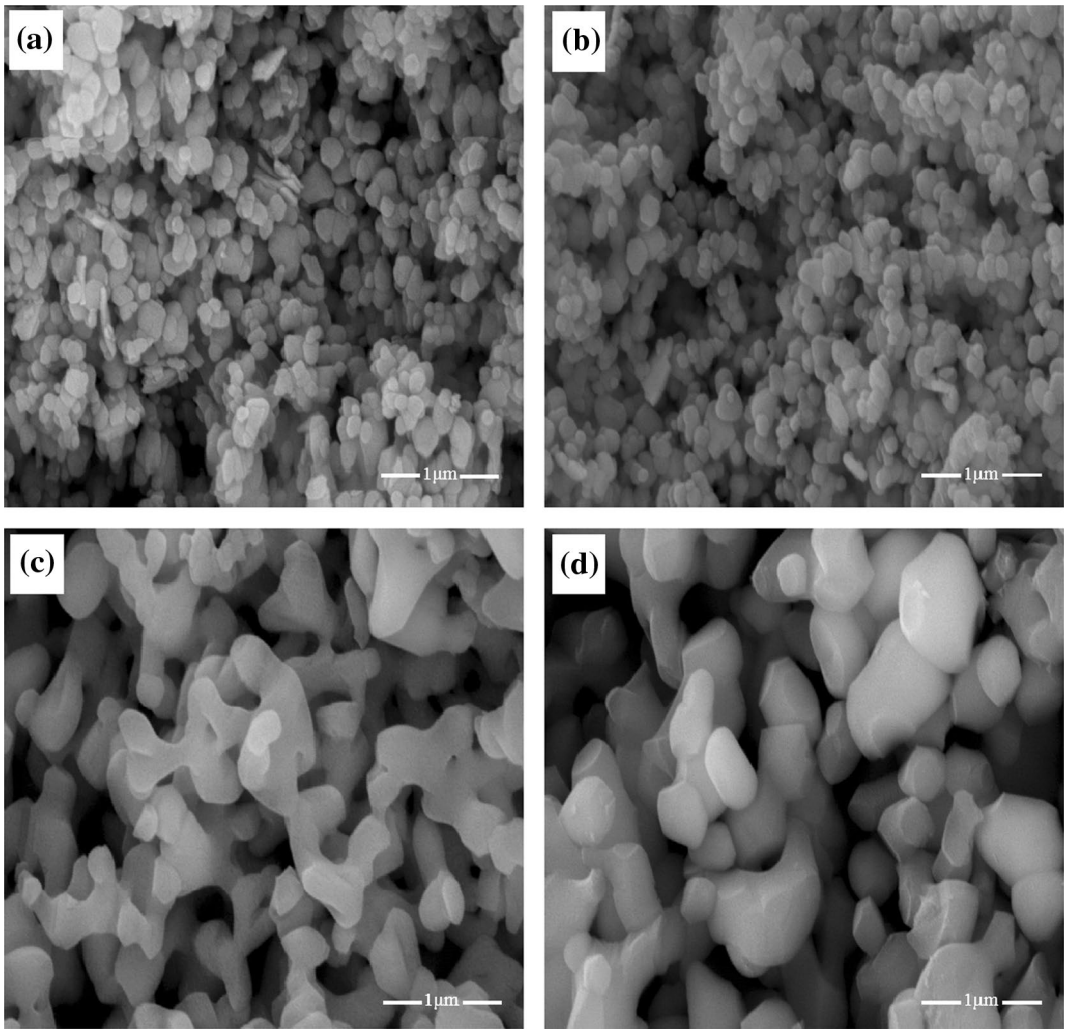

Fig. 5 Scanning electron micrographs (SEM) of **a** CCTO precursor and calcined samples for 2 h in air at different temperatures **b** 600 °C, **c** 800 °C and **d** 900 °C respectively. The micrographs have same magnification (×80,000) and scale bar length 1 μm

(JCPDS card No. 75-2188). In addition, following the orthorhombic phases of $CaTiO_3$ (JCPDS card No. 82-0228), tetragonal phase appeared as a secondary phase. And also observed some residuals of raw materials such as TiO_2 (JCPDS card No. 78-2486) and monoclinic phase CuO (JCPDS card No. 80-0076) agree with Guilleemet-Fritsch et al. [25]. The pure CCTO phase is obtained only when the ratio of calcium, copper and titanium are close to the stoichiometric ones.

XRD patterns of the powder calcined up to 800 °C show formation many of crystalline phase as $CaCu_3Ti_4O_{12}$ accompanied by extra sharp diffraction peak represented which indicates that some residuals of $CaTiO_3$ are existing at this stage. On the other side, XRD pattern of the powder calcined at 900 °C entirely exhibits pure $CaCu_3Ti_4O_{12}$ phase without any further phases; in this case, the $CaCu_3Ti_4O_{12}$ phase is formed at the expense of the secondary phases of $CaTiO_3$, CuO and TiO_2. The early formation of $CaCu_3Ti_4O_{12}$ at low temperatures is almost attributed to the highly energetic hydrothermal media of synthesis process in which the affinity to the formation of thermodynamically non-equilibrium products was significantly boosted aside from possessing smaller crystallite size of the powder, which introduced a broad surface area exposed to sequent reactions. Moreover, it is manifested that the perovskite structure of CCTO phase was formed at 900 °C [26] and the intensity of corresponding peaks displayed at 34.61°, 50.22° and 62.70° was considerably enhanced. The crystalline size (D) of the main line broadening peaks for calcined powder was calculated using Debye Scherrer formula

$$D = k\,\lambda/\beta\,\cos\theta \tag{3}$$

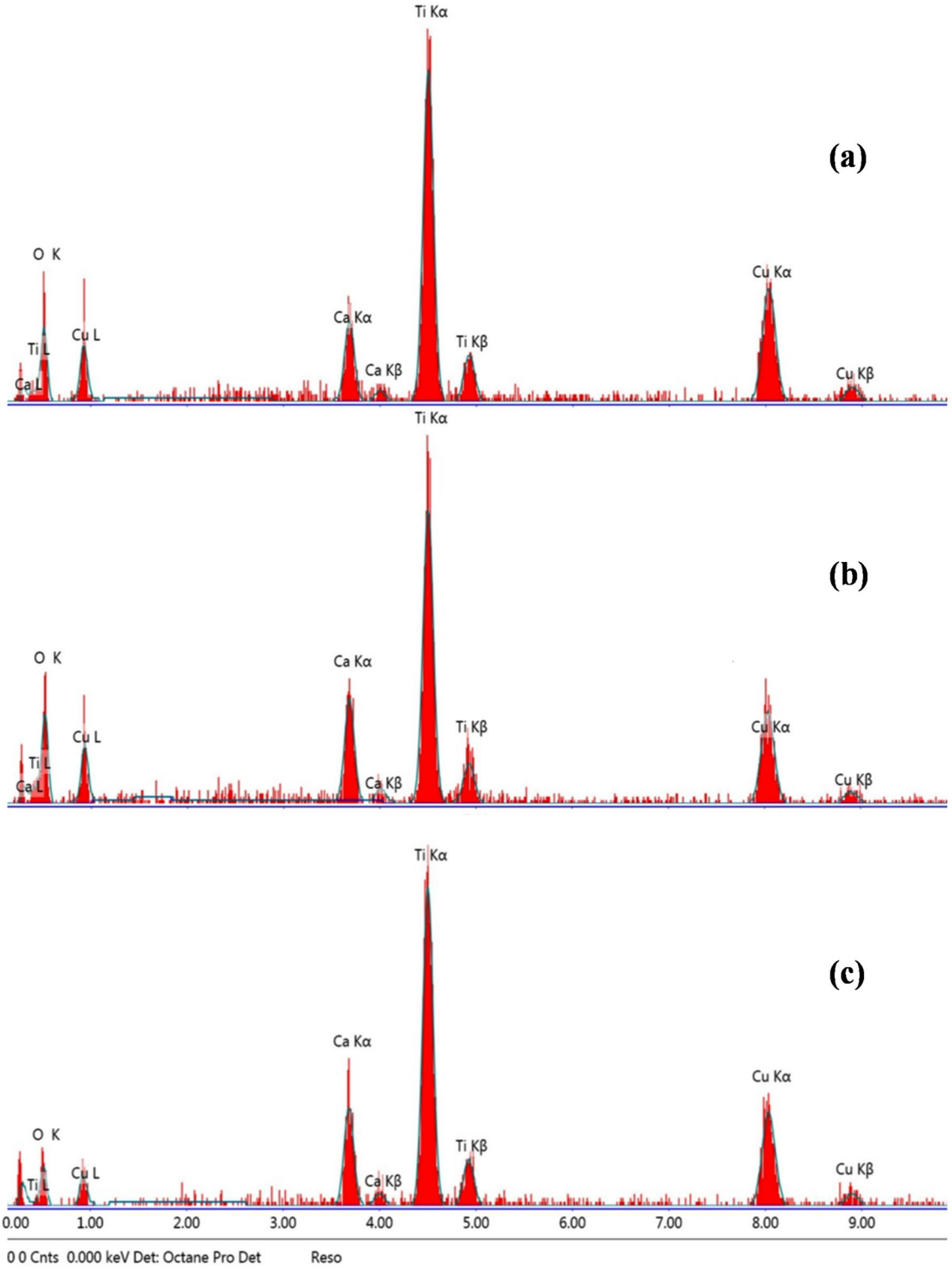

Fig. 6 EDX images for samples calcined of **a** as-prepared sample, at **b** 600 °C and **c** 900 °C, respectively

where k is a constant taken as 0.9, θ the diffraction angle, λ the wavelength of the X-ray radiation and β the full-width at half-maximum (FWHM) of each phase.

The obtained particle sizes for calcined powders at 600,700, 800, 900 and 1000 °C are 44.2 ± 14.5, 57 ± 18.4, 68.7 ± 20.6, 75.8 ± 12.9 and 80.2 ± 11.8 nm, respectively.

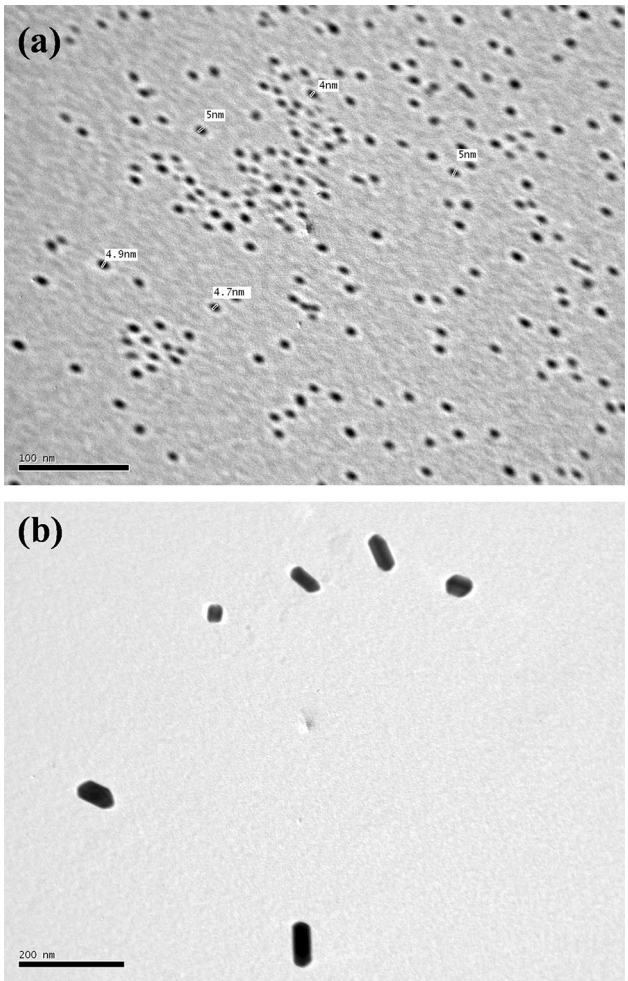

Fig. 7 High-resolution transmission electron microscope (HR-TEM) photographs of CCTO

The degree of crystallinity for all calcined powders estimated was ~ 54–68 using Materials Studio program. These results are totally compatible with TGA analysis discussed above and FTIR as will be debated in the following paragraph.

Figure 5a shows a homogeneous distribution of fine separated spherical species with small size in the as-prepared sample. However, Fig. 5b reveals that the sample calcined at 600 °C still has separated species of different phases. Obviously, the prepared CCTO powder has nano-crystalline structure, wherein the grain size enhanced by rising the calcination temperature. Furthermore, with increasing calcination temperature the separated species are compacted together and form large diffused profile as collapsed as in Fig. 5c,d. The average grain sizes of the as-prepared sample and calcined samples at temperatures (600, 800 and 900 °C) are 108, 109, 224 and 360 nm, respectively. Pure CCTO formed (at 900 °C) as seen in XRD, with a dense microstructure completely homogeneous morphology with abnormally large particles with smooth surfaces.

On the other hand, Fig. 6a–c shows the EDX spectrum of the region containing both large as well as small grains of CCTO ceramic. Ca, Cu, Ti and O are found to be 7.26, 20.17, 30.84 and 41.72% by weight for as-prepared powder and 7.98, 22, 32.32 and 37% 600 °C whereas the following ratios 6.52, 28.66, 29.06 and 35.66% are found at 900 °C, respectively. The oxygen loss confirms the formation of single phase of CCTO. This interpretation agrees well with XRD findings.

The influence of densification and calcination processes on microstructural features should be evaluated. Thereby, the microstructure of CCTO nanoparticles was further examined by high-resolution transmission electron microscope (HR-TEM) to acquire an evident insight of its characteristics. For instance, the morphology of the CCTO powder calcined at 900 °C was investigated and the photographs of HR-TEM reveal a nano-cubic crystal structure of $CaCu_3Ti_4O_{12}$ nanoparticles as clearly seen from Fig. 7. Moreover, the average size of the constituent particles is about 4.78 nm that is in good accordance with the formerly reported studies of these nanostructures [27]. The average particle size detected by HR-TEM is smaller compared to that calculated from XRD patterns. This is attributed to resolution difference in both techniques [28].

Furthermore, the corresponding selected area electron diffraction (SAED), which confirms highly oriented cubic crystal structure of the CCTO nanoparticles, is illustrated in Fig. 8a–d. However, Fig. 8d presents a single crystal structure, recognized as Kikuchi lines. It is formed due to thermal atom vibrations. Also, they existed when the selected area SAED is taken from single crystal region of the specimen. However, this structure plays a dominant role in improving dielectric properties of CCTO as will be discussed later.

The phase formation of CCTO was further confirmed by FTIR spectra of calcined powder at 800 and 900 °C, as shown in Fig. 9. The absorption peak at 458 cm^{-1} is due to Ti–O–Ti vibrational mode [29]. The peak observed at 532 cm^{-1} is related to bending vibration of Cu–O bond [30]. Absorption due to Ca–O was observed at 585 cm^{-1} [31]. There are absorption bands in the region 400–700 cm^{-1} arising from the mixed vibrations of CuO_4 and TiO_6 groups prevailing in the CCTO structure [30]. Spectrum of TiO_2 powder shows a wide absorption region between 450 and 930 cm^{-1}, with a shoulder at 550 cm^{-1}, and a weak peak at 1290 cm^{-1} [32].

The infrared spectrum of the CCTO has two main absorption envelopes in the region 400–900 cm^{-1} and 1300–1600 cm^{-1} as shown in Fig. 9. The broad band in the region ~ 400–900 cm^{-1} narrowed with increasing the calcined temperature. However, intensity of absorption band in the region ~ 1300–1600 cm^{-1} is decreased and gradually disappears with increasing calcination temperature. These variant results can be correlated by determining the area

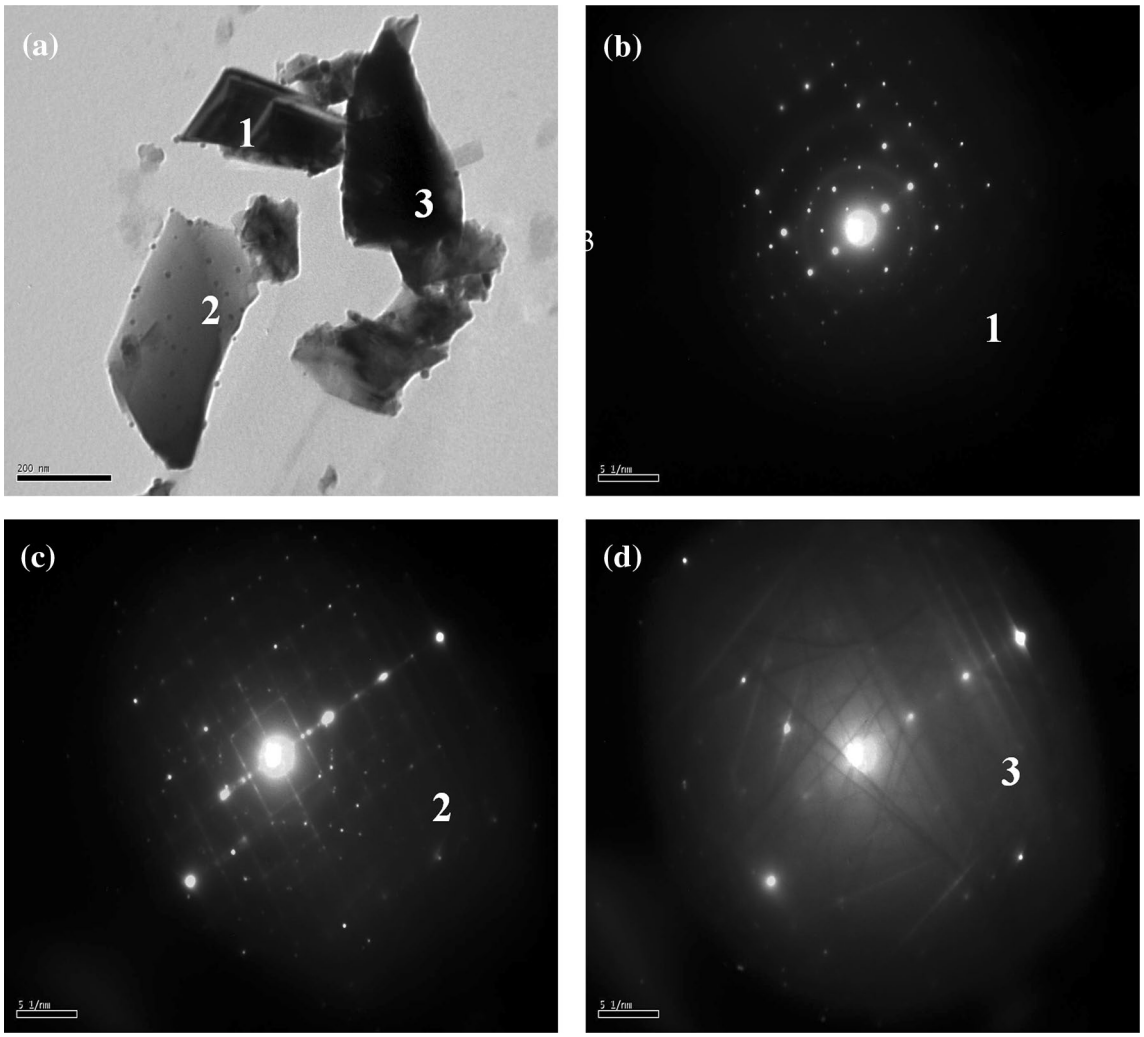

Fig. 8 Selected area electron diffraction (SAED) and diffraction patterns' photographs of CCTO

under the individual absorption regions in the plots. Figure 10 shows the relative area for two regions as a function of calcination temperature. There is decrease in the region ~ 1300–1600, and this region may be attributed to $CaTiO_3$, according to XRD; this phase disappears gradually with the increasing temperature. On the other hand, the region 400–900 cm^{-1} increases. The corresponding decrease and increase in the two regions are in the same rate. The IR result agrees well with XRD and SEM.

The modes of Raman for CCTO are observed at 444 cm^{-1}, 510 cm^{-1} and 576 cm^{-1} as reported in the literature [33]. In Fig. 10, there is a vibrational symmetrical mode and is detected below 200 cm^{-1} at room temperature 30 °C specifically at 154 cm^{-1}. This mode appeared due to TiO_2 of antenase origin. There are additional four remarkable Raman active modes for TiO_2 antenase with symmetries E_g, B_{1g}, A_{1g} and E_g observed at 154, 399, 520, and 641 cm^{-1}, respectively. The modes of $CaCO_3$ appear at 211 cm^{-1}, 808 cm^{-1} and 820 cm^{-1} [34]. The Cu–O stretch mode has been weakly appearance at 475 cm^{-1} [35].

In Fig. 11, after calcination at 600 °C for 2 h and after a careful observation, the intensity of TiO_2 decreased and broadened at 408 cm^{-1}, but it demolished at 520 cm^{-1}; this is a resultant of formation TiO_6 octahedral phase as well as Cu_2O phase at 66 cm^{-1} too [36]. With increasing temperature the $CaCu_3Ti_4O_{12}$ phase formed was increased and shift on expense of started precursors TiO_2, $CaCO_3$, CuO and a newly formed phase Cu_2O as shown at 800 °C, 900 °C and finally at 1000 °C. The increase in TiO_6 octahedral Raman active mode in CCTO ceramic structure at 506 cm^{-1} rather than other modes refers to the nanostructure of CCTO as referred in HRTEM microscopic graph which are less than 5 nm as a quantum dot structure [37].

The dielectric constant ε' and loss factor tan δ for CCTO are represented in Fig. 12 vs. frequency and at room temperature (30 °C). It is obvious that the values of ε' increased

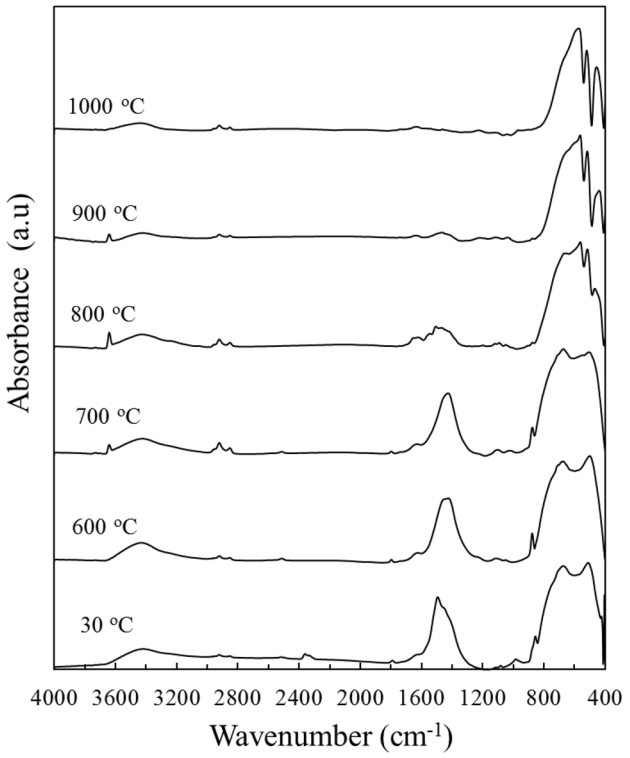

Fig. 9 FT-IR spectra of CCTO precursor and calcined samples for 2 h in air at different temperatures

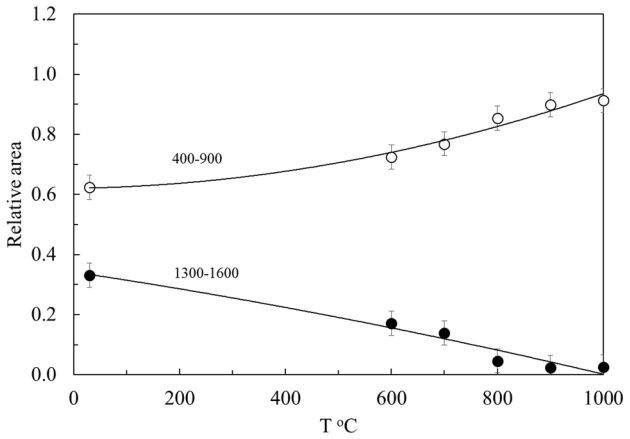

Fig. 10 Relative area CCTO precursor and calcined samples for 2 h in air at different temperatures

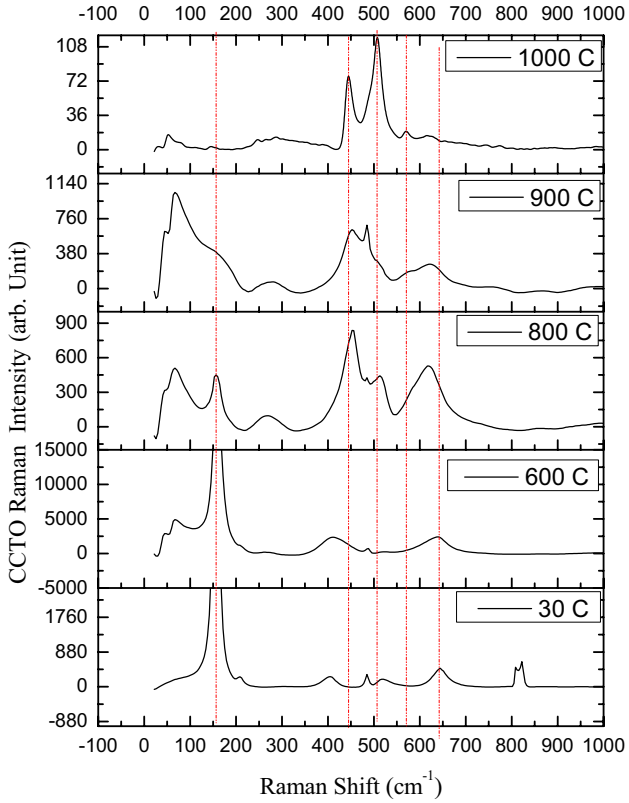

Fig. 11 Raman spectra of CCTO precursor and calcined samples for 2 h in air at different temperatures

with increasing calcination temperature up to 900 °C regardless the frequency value. ε' and tanδ rise sharply toward low frequencies. Moreover, the high dielectric constant ε' at low-frequency region suggests the possibility that the charge carriers accumulate at the interface of semiconducting grains and insulating grain boundary, which results in interfacial space charge polarization. However, the curves of tan δ vs. frequency have a broad relaxation. This relaxation can be explained by on the biases of the interfacial polarization or Maxwell–Wagner Sillars (MWS) [38].

On the other hand, right-side images of Fig. 13 demonstrate the change of the dielectric constant ε' and tan δ at fixed frequencies (1 Hz and 1 kHz) with calcination temperature. The obtained results in this figure revealed that the samples calcined at 800–900 °C have higher dielectric constant and lower loss compared to the other samples. This giant dielectric constant ε' is a clear indication of the formation of CCTO phase according to XRD results discussed previously. It can be also attributed to the dense microstructure of these samples. The "giant" dielectric constant value for ceramics with higher soaking time and temperature is mainly associated either with the presence of thin, reoxidized insulating grain boundary regions and large semiconducting grains or to a secondary phase at the grain boundaries [38, 39].

In addition, the semi-conductive nature of the grains (see Fig. 12) may arise from a small amount of oxygen loss during ceramic processing in air at elevated temperatures, as is known to occur in other titanate-based materials [5]. It is also reported that the grain and grain boundary microstructure greatly enhance the dielectric constant [40]. However, with increasing calcination temperature 900–1000 °C (right-side

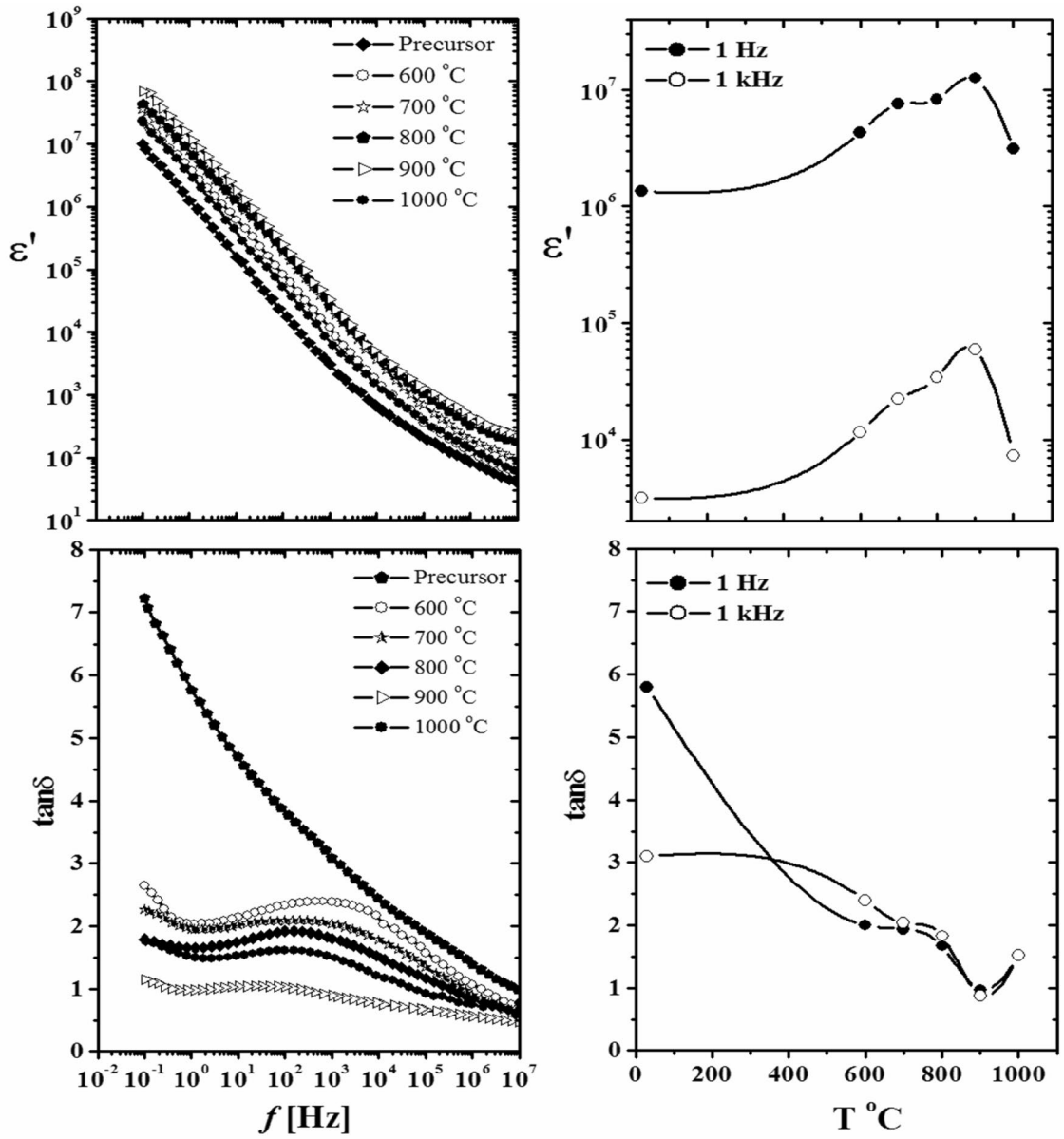

Fig. 12 Frequency dependence of permittivity ε' and loss factor tanδ for CCTO at 30 °C. The right-side images show the dependence data of ε' and tanδ for CCTO at 1 and 1 kHz on calcination temperature, respectively

images of Fig. 11) the values of dielectric constant ε' begin to decrease whereas the loss factor tan δ increases. This behavior refers to the deformation of CCTO cubic crystal structure as the samples begin to melt. This result is well supported by TGA results. So, it can be concluded that the optimum calcination temperature of CCTO prepared by this developed method must not exceed 800–900 °C.

5 Conclusion

In this work, $CaCu_3Ti_4O_{12}$ (CCTO) powders were synthesized by a modified sonochemical-assisted process. It is dried and calcined at relatively low processing temperatures and durations. The diffraction patterns show formation of

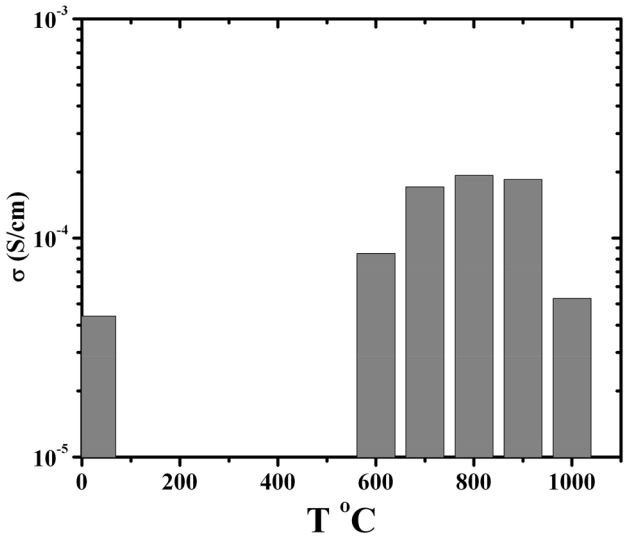

Fig. 13 Dependence of conductivity on calcination temperature

perovskite structure with the nano-sized crystallites of particle size ~ 4.8 nm. This very small particle size has not been reached before. Moreover, the dielectric results show a giant dielectric constant and lower values of loss factor for the samples calcined at 800–900 °C. For this reason, it is concluded that the optimum calcination temperature of the prepared CCTO must not exceed this temperature range. In addition, the prepared CCTO nanopowder is a promising material for energy storage applications.

Acknowledgement This project was supported financially by the Science Technology Development Fund (STDF) Egypt, Grant No. 15184.

References

1. K. Jong-Kuk, K. Nam-Kyoung, P. Byung-Ok, J. Mater. Sci. **35**, 4995–4999 (2000)
2. M. Afqir, M. Elaatmani, A. Zegzouti, A. Oufakir, M. Daoud, J. Mater. Sci. **31**, 3048–3056 (2020)
3. S.J.S. Flora, G. Flora, G. Saxena, Environmental occurrence, health effects and management of lead poisoning, in *Lead: Chemistry Analytical Aspects, Environmental Impact and Health Effects, Chap. 4*, ed. by S.B. Cascas, J. Sordo (Elsevier Science B.V., Amsterdam, 2006)
4. U.S. National Library of Medicine, TOXNET—Toxicology Data Network; HSDB—Hazardous Substances Data Bank; Barium Compounds, Accessed Nov. 4, (2015).
5. M.A. Subramanian, D. Li, N. Duan, B.A. Reisner, A.W. Sleight, J. Solid State Chem. **151**, 323–325 (2000)
6. J. Liu, C.G. Duan, W.N. Mei, R.W. Smith, J.R. Hardy, J. Appl. Phys. **98**, 093703-1–093703-5 (2005)
7. W. Li, R.W. Schwartz, Phys. Rev. B **75**, 012104-1–012104-4 (2007)
8. P. Lunkenheimer, V. Bobnar, A.V. Pronin, A.I. Ritus, A.A. Volkov, A. Loidl, Phys. Rev. B **66**, 052105-1–052105-4 (2002)
9. P. Lunkenheimer, R. Fichtl, S.G. Ebbinghaus, A. Loidl, Phys. Rev. B **70**, 172102-1–172102-4 (2004)
10. H.J. Hwang, K. Niihara, J. Mater. Sci. **33**, 549–558 (1998)
11. T. Ishii, M. Endo, K. Masuda, K. Ishida, Appl. Phys. Lett. **102**, 062901-1–062901-4 (2013)
12. P. Liu, Y. Lai, Y. Zeng, S. Wu, Z. Huang, J. Han, J. Alloys Comp. **650**, 59–64 (2015)
13. J. Liu, R.W. Smith, W.N. Mei, Chem. Mater. **19**, 6020–6024 (2007)
14. Z. Yang, Y. Zhang, R. Xiong, J. Shi, Mater. Res. Bull. **48**, 310–314 (2013)
15. S.M. Moussa, B.J. Kennedy, Mater Res B **36**(13-14), 2525–2529 (2001)
16. N. Wongpisutpaisan, N. Vittayakorn, A. Ruangphanit, Pecharapa W. **149**, 56–60 (2013)
17. Shengtao, L., Hui, W., Chunjiang, L., Yang, Y., Jianying, L.: Dielectric properites of Al-doped $CaCu_3Ti_4O_{12}$ ceramics by co-precipitation method. In: Proceed. Int. Conf. Electrical Insulating Materials (ISEIM), IEEE, pp. 23–26 (2011)
18. M.C. Sonia, P. Kumar, Process Appl. Ceram. **11**, 154–159 (2017)
19. M.M. Ahmad, E. Al-Libidi, A. Al-Jaafari, S. Ghazanfar, K. Yamada, Appl. Phys. A **116**, 1299–1306 (2014)
20. W.X. Yuana, S.K. Harka, W.N. Meib, J. Ceram. Process. Res. **10**, 696–699 (2009)
21. V. Saez, T.J. Mason, Molecules **14**, 4284–4299 (2009)
22. G. Cravotto, P. Cintas, Chem. Soc. Rev. **35**, 180–196 (2006)
23. G. Kianpour, M. Salavati-Niasari, H. Emadi, Ultrason. Sonochem. **20**, 418–424 (2013)
24. A. Aronne, M. Turco, G. Bagnasco, P. Pernice, M. Di Serio, N.J. Clayden, E. Marenna, E. Fanelli, Chem. Mater. **17**, 2081–2090 (2005)
25. S. Guillemet-Fritsch, T. Lebey, M. Boulos, Durand B. J. Eur. Ceram. Soc. **26**, 1245–1257 (2006)
26. S. Jin, H. Xia, Y. Zhang, J. Guo, J. Xu, Mater. Lett. **61**, 1404–1407 (2007)
27. S. Singh, S.B. Krupanidhi, Phys. Letter A **367**, 356–359 (2007)
28. S.A. Gad, G.M. El Komy, A.M. Moustafa, A.A. Ward, Indian J. Phys. **93**, 1009–1018 (2019)
29. P. Thomas, K. Dwarakanath, K. Varma, T. Kutty, J. Therm. Anal. Calorim. **95**, 267–272 (2008)
30. P. Thomas, K. Dwarakanath, K.B.R. Varma, T.R.N. Kutty, J. Phys. Chem. Solids **69**, 2594–2604 (2008)
31. T.B. Adams, D.C. Sinclair, A.R. West, Adv. Mater. **14**, 1321–1323 (2002)
32. H. Doweidar, K. El-Egili, R. Ramadan, M. Al-Zaibani, J. Non-Crystal. Solids **466**, 37–44 (2017)
33. A.F.L. Almeida, P.B.A. Fechine, M.P.F. Graca, M.A. Valente, A.S.B. Sombra, J. Mater. Sci. Mater. Electron. **20**, 163–170 (2009)
34. L. Bayarjargal, C.-J. Fruhner, N. Schrodt, B. Winkler, Phys. Earth Planet. Inter. **281**, 31–45 (2018)
35. M. Todaro, A. Alessi, L. Sciortino, S. Agnello, M. Cannas, F.M. Gelardi, G. Buscarino, J. Spectrosc. (2016). https://doi.org/10.1155/2016/8074297
36. N. Kolev, R.P. Bontchev, A.J. Jacobson, V.N. Popov, V.G. Hadjiev, A.P. Litvinchuk, M.N. Iliev, Phys. Rev. B **66**(13), 132102 (2002)
37. L. Singh, I.W. Kim, B.C. Sin, K.D. Mandal, U.S. Rai, A. Ullah, H. Chung, Y. Lee, RSC Adv. **4**(95), 52770–52784 (2014)
38. S.A. Gad, A.M. Moustafa, A.A. Ward, J. Inorg. Organomet. Polym. **25**, 1077–1087 (2015)
39. F.D. Morrison, D.C. Sinclair, A.R. West, J. Am. Ceram. Soc. **84**, 474–476 (2001)
40. J. Li, K. Cho, N. Wu, A. Ignatiev, IEEE Trans. **11**, 534–541 (2004)